Journal of Magnetism and Magnetic Materials 405 (2016) 317–323

Contents lists available at ScienceDirect

Journal of Magnetism and Magnetic Materials

journal homepage: www.elsevier.com/locate/jmmm

Electrically tunable spin polarization in silicene: A multi-terminal spin density matrix approach

Son-Hsien Chen

Department of Applied Physics and Chemistry, University of Taipei, No.1, Aiguo W. Road, Zhongzheng District, Taipei 10048, Taiwan

ARTICLE INFO

Article history:
Received 21 October 2015
Received in revised form
13 December 2015
Accepted 28 December 2015
Available online 12 January 2016

Keywords:
Silicene spintronics
Spin polarization
Spin–orbit coupling
Topological insulators
Spin field-effect transistor

ABSTRACT

Recent realized silicene field-effect transistor yields promising electronic applications. Using a multi-terminal spin density matrix approach, this paper presents an analysis of the spin polarizations in a silicene structure of the spin field-effect transistor by considering the intertwined intrinsic and Rashba spin–orbit couplings, gate voltage, Zeeman splitting, as well as disorder. Coexistence of the stagger potential and intrinsic spin–orbit coupling results in spin precession, making any in-plane polarization directions reachable by the gate voltage; specifically, the intrinsic coupling allows one to electrically adjust the in-plane components of the polarizations, while the Rashba coupling to adjust the out-of-plan polarizations. Larger electrically tunable ranges of in-plan polarizations are found in oppositely gated silicene than in the uniformly gated silicene. Polarizations in different phases behave distinguishably in weak disorder regime, while independent of the phases, stronger disorder leads to a saturation value.
© 2015 Elsevier B.V. All rights reserved.

1. Introduction

Spintronics devices of potential industrial applications rely on generating and manipulating spin polarizations particularly via electric means. Pristine graphene [1] is one of the early proposed topological insulators (TIs) [1–4] to create pure spin currents from quantum spin-Hall effect (QSHE) driven by the spin–orbit (SO) coupling (SOC) [1,5–7]. However, pristine graphene possesses very week intrinsic SOC [8–10] and lacks of adoptable band gap often required in semiconductor-based applications such as field-effect transistors (FETs). Thus, efforts are developing in searching and understanding hybrid graphene heterostructures [11,12] as well as other two-dimensional systems [13–16]. For example, graphene interacting with transition metal dichalcogenide [17–19] generates great interests. Compared to the pristine graphene, it was predicted that the QSHE exists with a three-order enhanced TI gap in hybridization with WS_2, WSe_2 [20], and $MoTe_2$ [21]. Experimentally, the MoS2-graphene heterostructure was demonstrated to function as a nonvolatile memory cell [22], and the graphene-WS2 heterostructure was performed with transparent and flexible substrate to act as a new generation of the FET of high ON/OFF ratio [23].

Another two-dimensional system attracting significant attentions is silicene [24–28], the silicon-based counterpart of graphene, sharing the same honeycomb structure but with lattice buckling [24,29]. The ubiquity of the silicon technology makes silicene a good candidate to be utilized in industrial applications [13–16]. Compared to graphene, pristine silicene not only has a larger intrinsic SOC [29] but also renders an electrically tunable [30,31] gap. Similar but richer characteristics [32,33] based on silicene were found. The quasi free-standing silicene was predicted to exist in a superlattice with hexagonal boron nitride [34], while strain in silicene effectively induces hole doping [35]. Using first-principles calculations, silicene decorated by transition metals were also investigated, predicting the existence of the quantum anomalous Hall state [36] and of different magnetic coupling between decorated and induced Si moments [37]; substantial energy gaps were found in heavy metal [38] as well as organic molecule [39] adsorption. Experimentally synthesized silicene has been realized [26–28]. Also noteworthily, recent studies have demonstrated that the silicene can serve as the FET [40,41] operable at room temperature; it is then intriguing to ask how silicene can be adopted for the spin FET [42], which essentially relies on grasping how different mechanisms in silicene alter the spin-polarizations, particularly, with all-electric means.

This paper presents an in-depth analysis of the spin polarizations based on the silicene spin FET structure. We examine how the polarizations of the outgoing spins, transported through gated silicene, would respond to the intricate but analyzable interplay of the applied electric field, magnetic field, intrinsic SOCs, and disorder. An overall picture, aiming at giving guidelines for realizing silicene-based electrically tunable polarizations, is given to comprehend the behaviors of the polarizations due to different mechanisms. The uniformly and non-uniformly gated silicene are both studied, while for simplicity we model the latter by two

E-mail address: sonhsien@utaipei.edu.tw

http://dx.doi.org/10.1016/j.jmmm.2015.12.088
0304-8853/© 2015 Elsevier B.V. All rights reserved.

opposite gate voltages. Without needing any magnetic fields, the latter gives a larger tunable range of the detected polarizations than the former by varying the gate or field boundary. Unlike in the case of absent Rashba SOC [43] where only diagonal elements of the spin-resolved conductance are required, we employ here a spin density matrix approach [44] capable of accounting for the spin-flip processes. We further impose the spin rotation enabling the formalism to deal with multi-terminal case containing any number of leads of arbitrarily injected spin directions. Especially, we examine the rarely discussed in-plane components of spin polarizations which commonly appear in the spin FETs.

2. Formalism

We begin with the generic tight-binding model of a buckled honeycomb lattice [29,45,43,32]

$$H = \sum_{i,s} u_i c_{is}^\dagger c_{is} - \gamma \sum_{\langle i,j\rangle,s} c_{is}^\dagger c_{js} + i\frac{\Delta_{SO}}{3\sqrt{3}} \sum_{\langle\langle i,j\rangle\rangle,ss'} \nu_{ij} c_{is}^\dagger \sigma_{ss'}^z c_{js'} + i\frac{2\Delta_R}{3} \sum_{\langle\langle i,j\rangle\rangle,ss'} \mu_{ij} c_{is}^\dagger \left(\vec{\sigma} \times \hat{d}_{ij}\right)_{ss'}^z c_{js'} + \Delta_S \sum_{i,s} \xi_i c_{is}^\dagger c_{js} + \Delta_Z \sum_{i,si} c_{is}^\dagger \sigma_{ss}^z c_{js}. \quad (1)$$

Here $c_{is}^\dagger$ (c_{is}) denotes the creation (annihilation) operator creating (annihilating) an electron of spin-z (with $s = \uparrow$ for spin-up and $s = \downarrow$ for spin-down) at site i, and $\vec{\sigma} = (\sigma^x, \sigma^y, \sigma^z)$ are Pauli matrices. The on-site potential u_i accounts for the clean (zero $u_i = 0$) and disordered (nonzero random u_i) systems, while γ represents the kinetic hopping between two nearest sites $\langle i, j\rangle$. The second and third lines in Eq. (1) take into account the intrinsic and Rashba SOCs through hopping between two next-nearest sites $\langle\langle i, j\rangle\rangle$ with strengths Δ_{SO} and Δ_R, respectively. Here sites $\langle\langle i, j\rangle\rangle$ are connected by the relative position vector $\vec{d}_{ij}$ with $\hat{d}_{ij} = \vec{d}_{ij}/|\vec{d}_{ij}|$. The time-reversal symmetry is preserved by assigning appropriate signs for $\nu_{ij} = +1\,(-1)$ if the hopping (from site i through a common site to site j) is anticlockwise (clockwise) and $\mu_{ij} = +1\,(-1)$ if the hopping is in sublattice A(B) as defined in Fig. 1. In the presence of the gate voltage by applying an out-of-plane E_z field in the z-direction perpendicular to the buckled x–y plane consisting of honeycomb A and B sublattices, the staggered potential $\Delta_S = lE_z$ ($\xi_i = +1$ for sublattice $i \in$ A and $\xi_i = -1$ for sublattice $i \in$ B) emerges via the

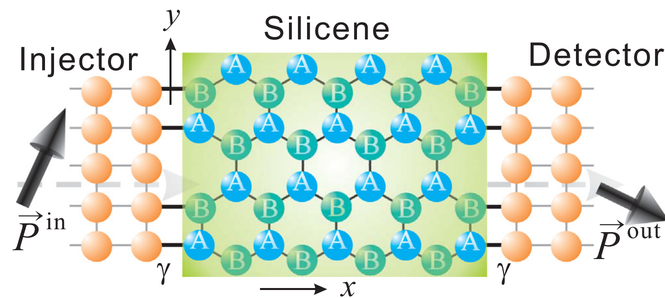

Fig. 1. Schematics of the device geometry. The injected spins of polarization $\vec{P}^{\,in}$ depart from the normal-metal injector, enter the silicene nanoribbon (buckled honeycomb of A and B sublattices), and then arrive with $\vec{P}^{\,out}$ (the spin polarization of the outgoing current) at the normal-metal detector. The solid lines connecting the semi-infinite injector/detector to the silicene represent the hopping γ between different materials.

last line in Eq. (1) with the buckling distance between A and B being l. The effective Hamiltonian equation (1) allows one to derive abundant phases that generally exists in the buckled honeycomb lattice. These phases include TIs, band insulators (BIs), spin-valley polarized metals (spin VPMs or SVPMs), marginal valley polarized metals of type 1 (MVPM1) and type 2 (MVPM2) as defined in Ref. [32].

For device geometry, we adopt the spin FET structure of a silicene zigzag nanoribbon with two terminals. As shown in the schematics Fig. 1, the silicene scattering region is in contact with two ballistic normal-metal (NM) leads labeled by $p=1$ (left) and $p=2$ (right). The left lead is the injector (source) from which electron spins are injected, while the right lead is the detector (drain) in which the polarization of the outgoing current is measured. The two NM leads are semi-infinite and are modeled by the square lattice with the Hamiltonian $-\gamma \sum_{\langle i,j\rangle,s} c_{is}^\dagger c_{js}$. Fig. 1 illustrates how the silicene couples to the two NMs through the hopping γ. The number of sites in a zigzag chain (N_x) and the number of zigzag chains (N_y) that form the honeycomb lattice determine the length and the width of the silicene, respectively. As an example, the silicene in Fig. 1 is of size $(N_x, N_y) = (9, 4)$. Note that the spin currents in the drain can be used to realize spin FETs with sending them to the filter of either parallel or anti-parallel magnetization. It should be noted that simply for simplicity of theoretical analysis, we choose the NM leads because the spin polarizations are preserved in NMs, while in realistic spin transistor applications the source and drain do not require being NMs.

We note that full spin polarization are described only via pure spin states, while mixed states are also needed to depict partial polarization often characterized by the ensemble statistics based on the density matrix rather than on a single wave function. We consider here the polarization of injected spins with the ensemble of $w_{\uparrow\theta_{in},\phi_{in}}$ proportion at the spin-up state $|\uparrow_{\theta_{in},\phi_{in}}\rangle$ and $w_{\downarrow\theta_{in},\phi_{in}}$ proportion at the spin-down state $|\downarrow_{\theta_{in},\phi_{in}}\rangle$. Here the up and down are defined with respect to the axis specified by the subscripts, polar angle θ_{in} and azimuthal ϕ_{in} in spherical coordinates. As an instance, $|\uparrow_{\pi/2,0}\rangle$ and $|\downarrow_{\pi/2,0}\rangle$ stand for the injected spins in directions $+x$ and $-x$, respectively. We reserve the notations $\uparrow$ and $\downarrow$ with the dropped ($\theta_{in} = \phi_{in} = 0$) subscripts for the spin-z up and down, namely, $\uparrow\,\equiv\,\uparrow_{0,0}$ and $\downarrow\,\equiv\,\downarrow_{0,0}$. The trace over the spin degrees of freedom of the density matrix $\rho^{in} = w_{\uparrow\theta_{in},\phi_{in}}|\uparrow_{\theta_{in},\phi_{in}}\rangle\langle\uparrow_{\theta_{in},\phi_{in}}| + w_{\downarrow\theta_{in},\phi_{in}}|\downarrow_{\theta_{in},\phi_{in}}\rangle\langle\downarrow_{\theta_{in},\phi_{in}}|$ yields the incoming polarization vector

$$\vec{P}^{\,in} = \mathrm{Tr}(\rho^{in}\vec{\sigma}). \quad (2)$$

For example, a full (100% polarization of $|\vec{P}^{\,in}| \equiv P^{in} = 1$) spin-$z$ injection consists entirely of $|\uparrow_{0,0}\rangle \equiv |\uparrow\rangle$ injected states, and thus $\rho^{in} = |\uparrow\rangle\langle\uparrow|$ gives $\vec{P}^{\,in} = (0, 0, 1)$; the proportion $w_{\uparrow\theta_{in},\phi_{in}} = w_{\downarrow\theta_{in},\phi_{in}} = 0.5$ represents the unpolarized injection, for one arrives at $\vec{P}^{\,in} = 0$ independent of the choices of θ_{in} and ϕ_{in}.

The ratio of the spin currents (I_{Sx}, I_{Sy}, and I_{Sz}) to the charge currents I_c in the detector signifies the spin polarization of the outgoing currents,

$$\vec{P}^{\,out} = \frac{(I_{Sx}, I_{Sy}, I_{Sz})}{I_c}. \quad (3)$$

Focus on the linear-response (low-bias) regime. Since the transmission $\boldsymbol{t}$ matrix determines all needed currents in evaluating Eq. (3), the matrix elements of $\boldsymbol{t}$ suffice to express the polarization $\vec{P}^{\,out}$. Particularly, the transmission probability,

$$T_{s',s} = \sum_{n,n'} |t_{n's',ns}|^2, \quad (4)$$

Download English Version:

https://daneshyari.com/en/article/1798292

Download Persian Version:

https://daneshyari.com/article/1798292

Daneshyari.com